Caving 2026 – A van As, D Cumming-Potvin & J Wesseloo (eds)

doi:10.36487/ACG_repo/2645_17

Evaluation of the impact of time-dependent compaction, induced stress and spacing on stability for deep cave mines

Miguel Fuenzalida [a,b,*], Pablo Paredes [c]

[a] *The University of British Columbia, Canada*

[b] *ITASCA, USA*

[c] *Newmont Corporation, Australia*

Abstract

In deep, high-column caving operations, the robustness and reliability of the extraction level is paramount to withstand the geotechnical challenges associated with higher stress. Larger-pillar footprint layouts offer potential advantages such as improved extraction level pillar stability and reduced development scope. However, these configurations can also reduce overall recovery, as the larger drawpoint spacing increases the height of the stagnant zones.

During cave establishment, isolated flow zones may form squat-shaped stagnant zones above drawpoint apices. If insufficient swell tonnage is extracted during undercutting, stagnant zones of broken material can persist between the top of the undercut and the extraction level, enabling transfer of high vertical stresses to the extraction level and increasing the risk of local instabilities. Additionally, as spacing increases, layouts may be more exposed to stress build-up from cave loads during extended draw cessation periods.

This study examines the influence of induced stresses and spacing on extraction level stability using an enhanced numerical modelling workflow that captures key mechanical processes in caved material, including time-dependent compaction, modulus softening/hardening and rock mass strength degradation. Two footprint configurations (32 × 20 m and 35 × 22 m), two production ramp-up strategies and two rock mass strength conditions (moderate and weak) were assessed.

Results indicate that the larger-pillar layout generally improves extraction level stability compared to the narrower configuration. However, increased vertical stress from time-dependent compaction during draw cessation can lead to localised instabilities in weaker rock masses, even for the larger-pillar layout case. These findings highlight the need to balance layout spacing and production scheduling to manage stress evolution and maintain long-term extraction level performance.

Keywords: *footprint stability, cave mining, induced stress, numerical modelling, time-dependent compaction*

1 Introduction

Induced stresses and associated compaction are key variables in the performance and stability of the extraction level during cave establishment and cave propagation. Understanding these effects is essential when evaluating extraction level configurations.

In the context of deep, high cave columns, larger-pillar layouts offer advantages, primarily due to allowing the following:

* Corresponding author. Email address: mfuenzalida@oneitasca.com

- improvement in the extraction level pillar stability during cave establishment with increased pillar dimensions, reducing the risk of life-altering injuries or fatalities from rockfalls as a result of pillar bursting
- improvement in the effectiveness of drawpoint bunding as a critical control for inrush hazards, particularly during late-stage cave production, by increasing the drawpoint apron length
- development scope reduction and associated benefits.

One of the downsides of increasing spacing to achieve larger pillars is the reduction in recovery compared to narrower layouts. Flow modelling shows that increasing the spacing increases the height of the stagnant zone (volume of broken but unmobilised material above the extraction level apices) and hence the amount of unrecovered material (Castro 2006; Castro et al. 2012; Paredes 2022). As column heights increase, models show the proportional recovery loss reduces. However, the extent of the recovery loss and its impact will depend on several other factors, including effective draw strategy and management, rock mass characteristics and geotechnical environment, grade distribution, metal prices, and operating and capital costs. Also, flow models have limitations in terms of the mechanisms they can reproduce, including the effects of compaction and associated porosity changes. They also tend to be performed under idealised draw conditions. Therefore, detailed analysis, modelling and risk assessments need to be performed for the specific conditions of a given project before selecting the extraction level layout.

Additionally, the following other key vulnerabilities associated with increasing spacing are noted:

- **Stronger dependence on uniform and continuous draw**: given increased spacing increases the height from which mass flow is formed (height of interaction zone), a higher portion of the column is subject to differential draw and shearing. Therefore, the risk of fines generation and inrush susceptibility increases, making the application of stringent draw control even more relevant.
- **Reduced footprint productivity and system redundancy**: as spacing increases, fewer drawpoints and drives are available to maintain the production capacity, which makes the larger-pillar layouts less productive on a square metre basis and more susceptible to planned and unplanned drive downtime. This further compounds the vulnerability associated with a stronger dependence on uniform draw.
- **Greater sensitivity to draw interruptions and downtime**: draw interruptions cause vertical stress to increase on the extraction level pillars. For larger-pillar layouts when a drawpoint or extraction drive needs to temporarily cease extraction for operational or maintenance reasons, there is less chance of isolated movement zones from surrounding drawpoints intersecting higher in the column over this area (and shedding cave loads away) and therefore a higher likelihood of the shut area attracting high cave loads.
- **Higher undercut and connectivity requirements**: as drawpoint spacing increases, undercut height should be assessed to ensure continuous void formation, avoid remnant pillars and prevent point loading on extraction level pillars (Morales et al. 2024). To improve the efficiency of blasting and pillar geometry and assist airgap generation by allowing the material to flow directly to the drawbell, the angle of flow should be taken into consideration when scaling the design variables linked to drawpoint spacing to promote healthy consistent undercut generation early in the extraction of the drawpoint, as illustrated in Figure 1. Additionally, the draw strategy during the undercutting process needs to ensure enough void is being generated as the sequence progresses to ensure a healthy initiation of the caving process.

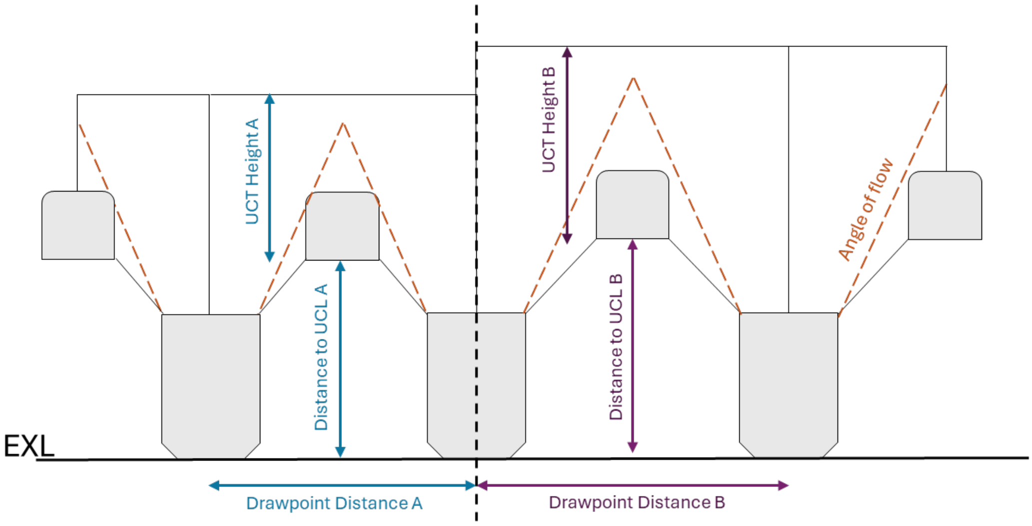

Figure 1 Illustration of interrelated design variables for (a) narrower spacing design and (b) wider spacing: drawpoint distance, distance between levels, undercut height and relationship with angle of flow

- **Increased likelihood of large stagnant zones forming during undercutting and cave establishment**: a key challenge associated with larger-pillar layouts is the increased likelihood of large stagnant zones persisting between flow zones during undercutting and cave establishment. During the drawpoint ramp-up period, flow zones are relatively immature and therefore narrow and isolated (non-overlapping), resulting in stagnant material (volume of broken/blasted but unbulked and unmobilised material) above the major apices. If swell tonnage is inadequately drawn during undercutting, columns of broken material connecting the undercut and extraction level may persist during cave propagation. These volumes are relatively stiff and able to transmit substantial vertical stresses through the undercut to the extraction level, potentially leading to unanticipated stability issues.

Evidence of the above mechanism was provided by the partial collapse of Henderson mine's 615 drift at the 7700SW panel, where vertical stresses were transferred through the undercut level, impacting the stability of an extraction drive (Shea et al. 2018). Additionally, stagnant zones and point loading on major apices during undercutting can cause significant compaction of the broken rock, as shown in Figure 2. This image shows a collapsed zone in the same drift, showing highly compacted broken rock with decreased porosity, a well-graded size distribution, and increased strength due to void space reduction and increased apparent cohesion (Shea et al. 2018). This mechanism has also been observed following cessation of mining (Kwok & Pierce 2011) as well as when drawpoints remain inactive for extended periods due to unexpected drift closures (Cancino et al. 2022).

Time-dependent recompaction is a widely recognised phenomenon in civil engineering, akin to observations in caving mines. For example, rockfill dams demonstrate settlement and deformation under constant loads over extended periods (Oldecop & Alonso 2007). Understanding the effect of static and time-dependent compaction in gravity flow and induced stresses is particularly relevant for scenarios where draw has ceased for long periods of time and there is potential for production restart or establishment of blocks below this recompacted material. It is also relevant to assess scenarios where draw-induced loads could affect the long-term stability of critical infrastructure inside the footprint. However, current numerical modelling workflows do not comprehensively integrate the effects of static and time-dependent compaction. These workflows often focus on specific stages of the caving process, failing to capture cumulative performance across all stages. Addressing this gap is crucial for advancing the predictive capabilities of numerical models in block cave mining. Thus, this work aims to investigate the effect of stress, compaction and spacing in high-column caves throughout the different stages of the life of the extraction level, specifically assessing:

- stress build-up and extraction level pillar response during cave establishment
- extraction level pillar response to draw cessation events.

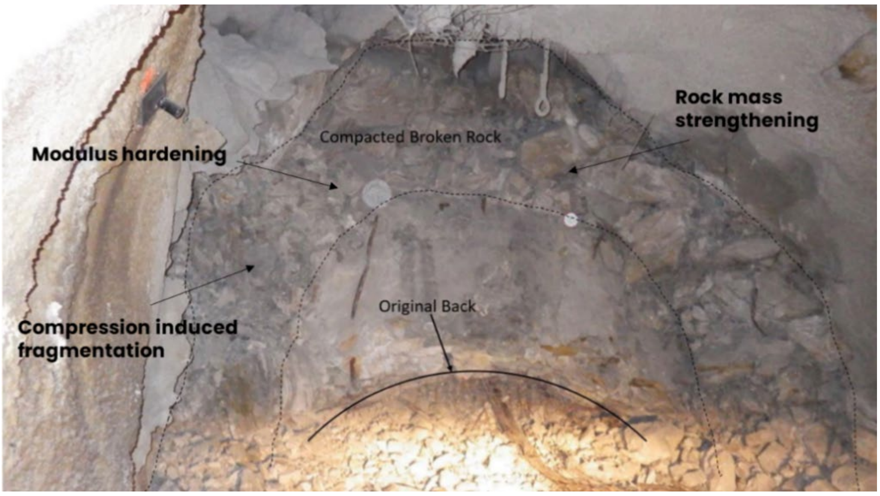

Figure 2 Exposure of compacted fragmented rock after tunnel collapse at Henderson mine (modified from Shea et al. 2018)

2 Approach

In this study, the FLAC3D-MassFlow coupled methodology (Fuenzalida et al. 2018) was used to investigate the impact of stress and compaction on recovery and stability within the context of wide drawpoint layouts. This approach allows one to track the redistribution of stress as material is extracted from the drawpoints (as shown in Figure 3). The hybrid FLAC3D-MassFlow approach simulates the caving process by explicitly modelling each isolated movement zone derived from MassFlow in FLAC3D to determine the yielded zone, cave back and airgap associated with mass drawn. After one cycle of extraction, MassFlow reports the location of the movement zones and the presence of air (if present) to the continuum FLAC3D model. FLAC3D solves stresses associated with the presence of these zones and estimates the yielded zone surrounding the cave. FLAC3D then informs MassFlow which zones (initially inactive) could now be mobilised. The procedure is repeated until the draw schedule, used as an input to MassFlow, is completed.

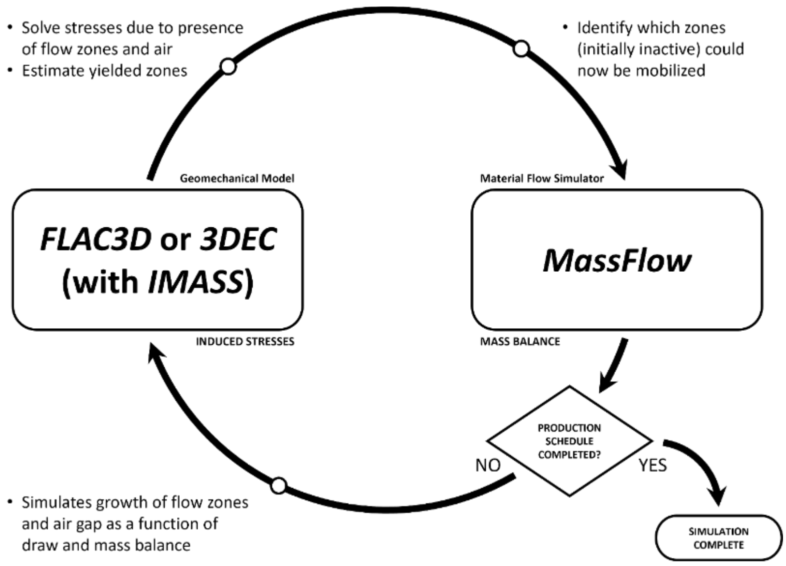

Figure 3 Conceptual scheme of the coupled FLAC3D-MassFlow approach (Fuenzalida et al. 2018)

The IMASS constitutive model (Ghazvinian et al. 2020), which is integrated into FLAC3D, was used during this study, as it can comprehensively characterise the various processes experienced by the rock mass during material extraction. These processes can be classified as rock mass weakening/strengthening, static modulus softening/hardening, compression-induced fragmentation, and time-dependent compaction.

2.1 Rock mass weakening/strengthening

Damage, disturbance and the associated loss of strength (i.e. weakening) are captured in two phases in IMASS. During Phase 1, damage is the result of fracturing of the intact rock due to stress changes. This causes a small (negligible) increase in porosity, as most of the damage is associated with the accumulation of plastic shear strain. Once the rock mass reaches a 'critical' plastic shear strain, Phase 1 ends and its strength is equal to the 'post-peak' strength. During Phase 2, additional deformation and disturbance as a result of the rearrangement of rock blocks cause a significant increase in porosity and permeability. The loss of strength (and modulus) depends on the volumetric strain increment (VSI), i.e. bulking factor. Once the rock mass reaches a state of maximum volumetric strain, Phase 2 ends and the rock mass reaches the 'ultimate' residual strength. If stresses are shed back onto fully bulked regions (e.g. in the case of ceased draw), VSI will decrease and the rock mass will strengthen, transitioning from the weaker 'ultimate' residual strength to the stronger 'post-peak' strength. A detailed description of the IMASS constitutive model is given in Section 3.1.2.

2.2 Static modulus softening/hardening

As the rock mass yields via shear or tension, it also experiences bulking and the associated drop in modulus (i.e. softening). Representation of this softening mechanism is required to properly capture how new loads are distributed within the bulked regions. Softening in IMASS considers the results of laboratory testing by Pappas & Mark (1993), which show that the modulus of rock drops in a nonlinear fashion with increased bulking and that the rate of modulus change is a function of fragment shape and intact strength (Figure 4). IMASS also allows the reverse process, in which a fully bulked rock mass would recompact (decrease in VSI), allowing for modulus hardening. To demonstrate this, a single zone oedometer test was carried out using the IMASS constitutive model by testing different degrees of initial bulking (VSI) and intact rock strength. The results of this test are shown in Figure 5. The results show that loose (higher initial VSI) rock compacts more than dense (lower initial VSI) rock for the same vertical load (σ_{zz}) and that weaker rock compacts more than strong rock for the same vertical load (σ_{zz}). These results agree with the published laboratory oedometer tests conducted on carbonate and silica sands (McDowell & Bolton 1998).

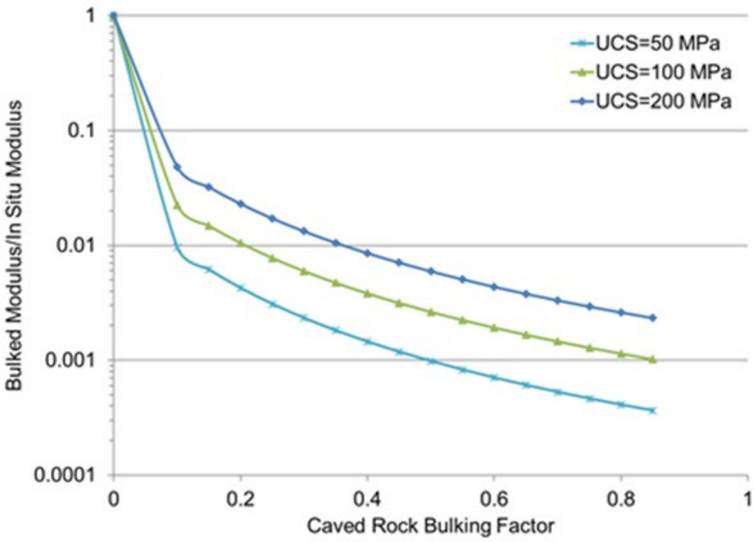

Figure 4 Bulk modulus/in situ modulus ratio as a function of bulking factor and intact strength, after Pappas & Mark (1985)

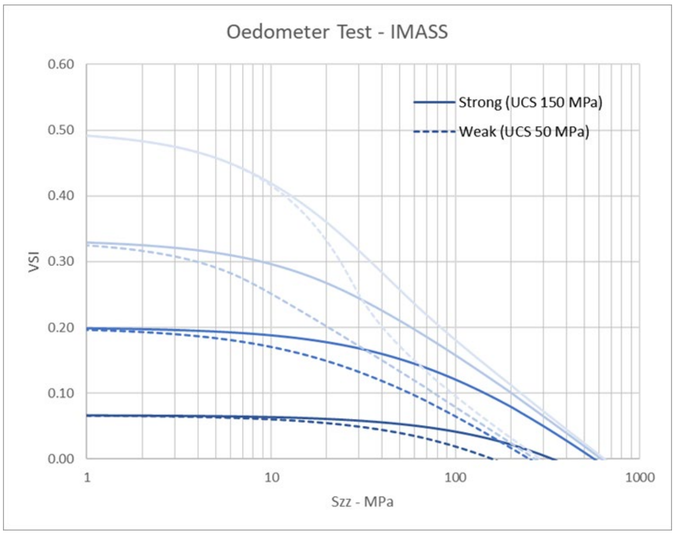

Figure 5 Example of a single zone oedometer test using IMASS constitutive model

2.3 Time-dependent compaction

Oldecop & Alonso (2007) provide a time-dependent compressibility index (λt) based on their large-diameter (300 mm) one-dimensional compression (odometer) experiments on specimens of rockfill-type material, a crushed slate with a maximum particle size of 40 mm. The empirical data shows time-dependent strain data as a function of applied stress and different constant suction values, which is inversely proportional to relative humidity (Figure 6). These empirical data can be used to approximate the time-dependent compaction in cave mining by including the effects of particle size, size distribution, particle strength and particle shape. The following relationship can be established:

$$\lambda t = d\varepsilon / d(\ln t) \tag{1}$$

where:

$d\varepsilon$ = strain increment

T = time elapsed since the application of the last load increment.

This equation is useful for a rough estimate of caved rock settlement as well as investigating the factors that affect the settlement rate. Values of λt are plotted for various vertical stresses in Figure 6. Although there is some scatter in the data, it is clear that the applied stress and total suction (a function of fragment saturation) are two controlling factors of λt.

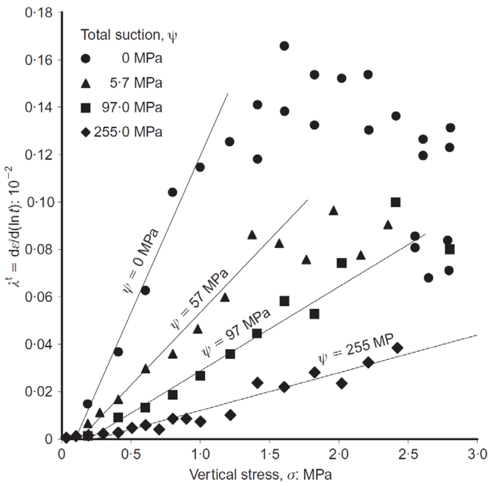

Figure 6 Time-dependent compressibility index against applied stress for different constant suction values (Oldecop & Alonso 2007)

Kwok & Pierce (2011) indicate that particle breakage is likely to be the dominant mechanism causing time-dependent deformation in caved rock. They also suggest that time-dependent particle breakage is generally a result of a stress corrosion mechanism acting to extend cracks in the particles. The stress corrosion mechanism is dependent on stress, mineralogy, geometry, time and the presence of water.

To apply the experimental results of Oldecop & Alonso (2007) to a cave-scale model, two scaling factors are introduced to adjust the compressibility index obtained from those experiments: intact rock strength and cave load. The rock block strength (RBS) accounts for the assumed intact rock strength in the model while incorporating scale effects for rock blocks of approximately 1 m in size. This scaling assumes that the intact uniaxial compressive strength (UCS) used in the model is reduced by a factor of 2.5. Meanwhile, the vertical cave load (σ_zz) is an emergent property of the model.

The time-dependent strain difference (or differential bulking factor), after incorporating caved rock properties and cave-induced loads, is computed using the following equation:

$$\Delta\varepsilon = \frac{\sigma_{v_{cave}}}{RBS_{1m}} * \frac{UCS_0}{\sigma_{v0}} * \lambda_0 * ln(days)$$

where:

σ_{v_cave}	=	cave load (MPa)
RBS_{1m}	=	rock block strength (MPa)
UCS_0/σ_{v0}	=	20.5
λ_0	=	compressibility index ($1.2e^{-3}$ for Pancrudo slate under saturated condition).

3 Numerical model

To evaluate the effect of spacing on the response to induced stresses in the extraction level during cave establishment, considering static and time-dependent compaction, two footprint layout configurations (Figure 7) were analysed, with both layouts covering an area of approximately 100,000 m² (~320 × ~300 m):

1. **Base case layout** representing a current configuration in high-column cave mines, with drawpoint spacing of 32 × 20 m and a total of 320 drawpoints.
2. **Larger-pillar layout** representing an increase of approximately 10% in both drawbell drive and extraction drive spacing, for a total of approximately 20% increase in drawbell tributary area, i.e. drawpoint spacing of 35 × 22 m and a total of 270 drawpoints.

The base case layout used a draw schedule based on the production rate curves (PRCs) depicted in Figure 8. For the larger-pillar case layout, two draw schedules with different PRCs were evaluated. The first draw schedule (35 × 22 m base case) used the same draw rate on a drawpoint basis (tpd/drawpoint) as the base case (32 × 20 m layout), while the second draw schedule applied a draw rate proportional to the larger area of influence representative of the 35 × 22 m layout (i.e. used the same PRC from the 32 × 20 m case on a t/m^2/day basis), resulting in a 20% higher draw rate on a drawpoint basis (t/dp/d).

The draw schedules were modelled using weekly periods. During the first week, a drawpoint became active in the model and drawbell tonnage was extracted. Additionally, 30% of the undercut tonnage (equivalent to 1.5 times the swell) was extracted during weeks 7–9 of each drawpoint (i.e. undercutting occurring approximately 6 weeks after drawbells are fired). A post-undercut strategy was followed, with a lead-lag of one drawbell and an undercut advance rate of 6 drawbells per month.

Each drawpoint was assumed to extract at a rate of 0.1 t/m²/day until a hydraulic radius of 25,000 m² was reached.

To evaluate the impact of time-dependent compaction, the draw was interrupted for one month in the central extraction drive after 200 weeks of continuous extraction (once the cave had reached an equivalent height of approximately 600 m); after this month, the draw was resumed. The 600 m height was selected since beyond ~600 m, cave loads are not expected to significantly increase due to the effect of stress arching of the caved material column (Pierce 2018).

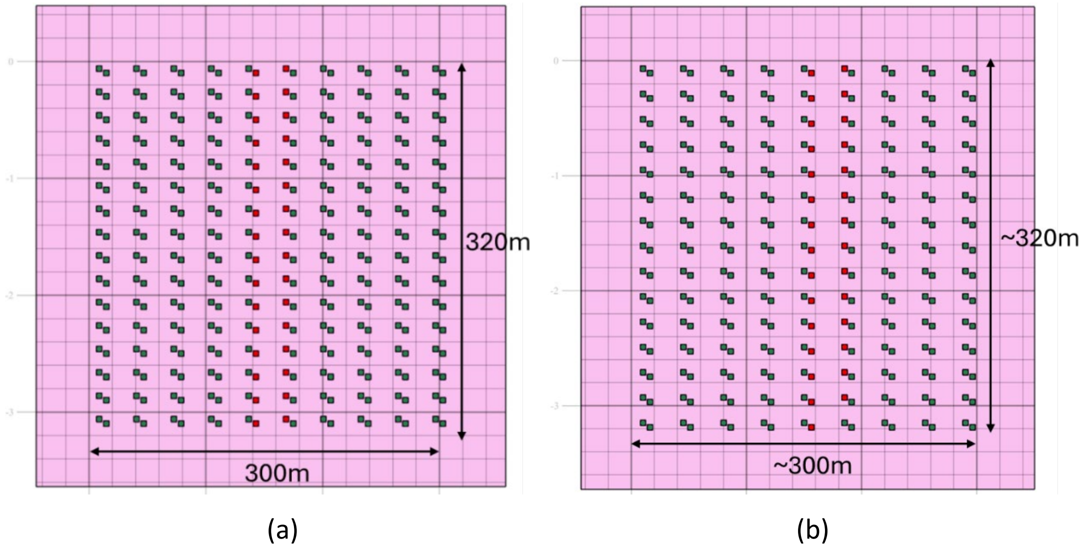

Figure 7 (a) Base case layout: 32 × 20 m; (b) Larger-pillar layout: 35 × 22 m. The central extraction drive is interrupted once the cave has grown to an equivalent height of approximately 600 m (red drawpoints)

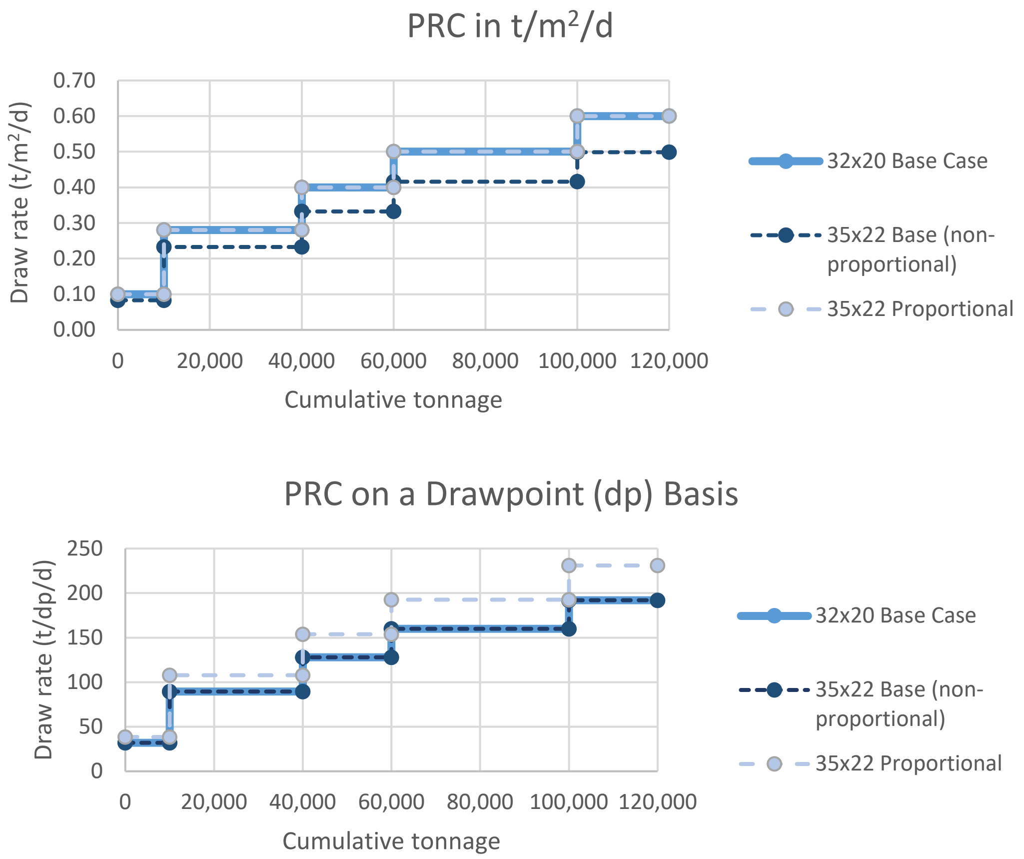

Figure 8 Production rate curves per drawpoint and by t/m²/d for base case and proportional draw schedule

The material properties used as inputs in the model are summarised in Table 1. The base case uses a moderate rock mass strength. An alternative case was also studied in which the rock mass strength is half the rock mass strength of the base case (i.e., weak rock mass strength.)

Table 1 Material properties used in the model

Material property	Rock mass strength	
	Moderate	**Weak**
Intact uniaxial compressive strength (Pa)	70e6	35e6
Geological strength index	65	65
Hoek Brown parameter: m_i	20	20
Intact Young's modulus (Pa)	40e9	40e9
Maximum bulking factor (VSI)	20%	20%

The footprint was assumed to be located approximately 1,200 m below the ground surface, reflecting a high-column cave condition.

The in situ stress conditions used for base case numerical models were:

- vertical Sig3 (magnitude gradient 0.027 MPa/m depth)
- horizontal Sig1 with trend north–south (kh of 1.8)
- horizontal Sig2 with trend east–west (kh of 1.2).

The simulated cases are summarised in Table 2.

Table 2 List of cases simulated

Case	Layout	Draw schedule	Rock mass strength
1	32 × 20 m	Base	Moderate
2	35 × 22 m	Base	Moderate
3	32 × 20 m	Base	Weak
4	35 × 22 m	Base	Weak
5	35 × 22 m	Proportional	Moderate

4 Results and discussion

4.1 Footprint-induced stress and damage

The stress evolution in the extraction level as cave establishment and extraction progress can be categorised into four stages (Figure 9):

1. Pre-mining stress: the initial in situ stress conditions before mining begins.
2. Abutment loading: elevated stress concentration affecting the footprint ahead of the cave during cave establishment.
3. Relaxation due to cave transition: a reduction in stress as the cave grows over the footprint during cave establishment and propagation.
4. Cave loading: stress redistribution based on cave self-weight once the cave is fully matured, influenced by draw control during interruptions and considerations of time-dependent effects.

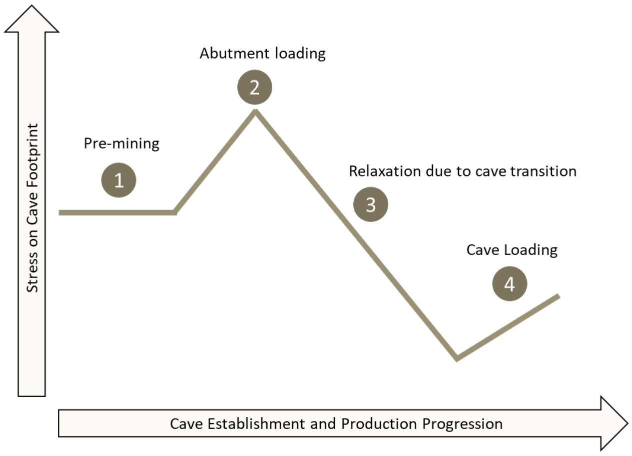

Figure 9 Stages experienced during loading cycle at a cave footprint layout

The stability of the extraction level in cave mining must be assessed throughout the different stages of mine life, not just during the peak of stress abutment, as pillar stability is affected by evolving induced stresses. As the cave develops and matures with increased production, induced stress changes in both magnitude and orientation.

Figures 10 and 11 illustrate how the major principal stress (σ_1) evolves on the footprint throughout cave establishment (Stages 1 and 2) and subsequent propagation and maturity (Stages 3 and 4).

In Stage 1, stress levels remain moderate because only the extraction and drawpoint drives have been developed. As the cave advances southward, the abutment zone grows and induced stresses increase, reaching their maximum in Stage 2.

When the cave extends beyond the footprint in Stage 3, stresses begin to relax and redistribute outward. In Stage 4, stress levels increase again but remain well below the Stage 2 peak; at full maturity, cave self-weight is carried primarily through vertical point loading on the major apices.

This loading cycle causes progressive pillar damage, and depending on pillar strength and geometry, the evolving stress conditions over the mine's life may result in varying levels of infrastructure impact.

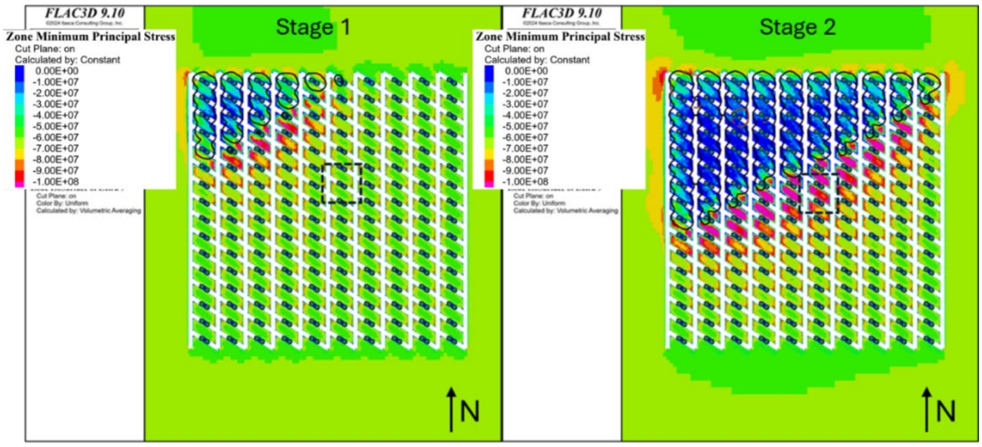

(a) (b)

Figure 10 Major principal stress (Pa) Sig1 from 0 (blue) to 100 MPa (pink) on footprint during cave establishment. Stage 1 (a) and Stage 2 (b) stresses are highlighted using the black square – 32 × 20 m layout

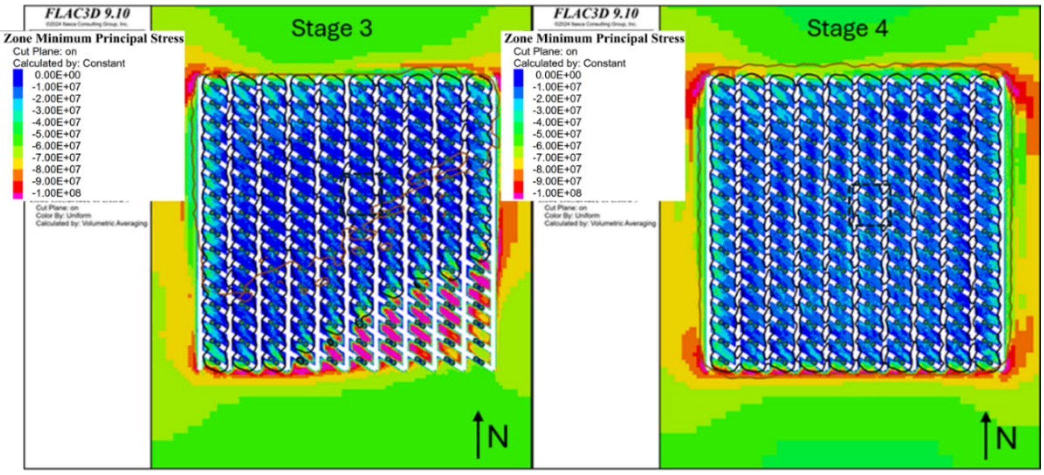

(a) (b)

Figure 11 Major principal stress (Pa) Sig1 from 0 (blue) to 100 MPa (pink) on footprint during and after cave matures. Stage 3 (a) and Stage 4 (b) stresses are highlighted using the black square – 32 × 20 m layout

Serviceability and performance of the extraction level during the life of mine were assessed explicitly by representation of tunnel excavations in the FLAC3D-MassFlow coupled caving model. Strength loss (sloss) was used as the damage indicator in the IMASS constitutive model. This parameter changes between 1 and −1 for various degrees of damage to the rock mass, as follows:

Between peak and post-peak envelopes, sloss changes between 1 and 0:

$$sloss = 1 - \frac{plastic\ shear\ strain}{critical\ plastic\ shear\ strain}$$

Between post-peak and ultimate strength envelopes, sloss changes between 0 and −1:

$$sloss = -\frac{volumetric\ strain}{maximum\ allowable\ volumetric\ strain}$$

Figure 12 schematically represents sloss for different degrees of damage in a rock mass:

- Between 'B' and 'C', the damage to the rock mass is due to fracturing of intact rock, resulting in progressive cohesion weakening and mobilisation of the friction angle.
- At 'C' (sloss = 0), the rock mass is assumed to have undergone fracturing, but the resulting rock fragments are still fully interlocked (cohesion in the rock mass is completely lost, but friction is high). Near excavation surfaces, if sloss reaches zero (tensile and cohesional strength are fully lost), unsupported rock would unravel (Kaiser 2019), making sloss = 0 an indicator for estimation of depth of failure. That said, experience has shown that the underground openings can remain stable with support even after complete loss of cohesion, as long as the support is sufficient to retain the failed material. Support capacity will be consumed where the rock is most vulnerable to bulking with further stress changes. For this reason, sloss < −0.15 (15% or more of bulking potential achieved) was adopted as a conservative indicator of bulking depth.
- At 'D', the degree of rock fragments interlocking is at its minimum, and the porosity is maximised (rock mass is fully bulked). Unlined shafts or minimally supported drives at this state are considered unserviceable.

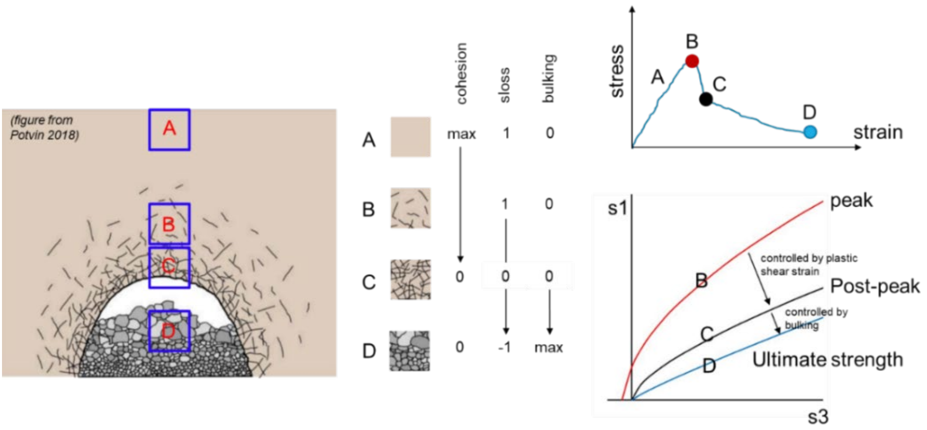

Figure 12 Schematic representation of sloss for various degrees of damage in a rock mass. Figure modified from Cumming-Potvin et al. (2018)

Figure 13 shows sloss contours for the moderate strength case at the end of Stage 4 for the 32 × 20 m (Figure 13a) and 35 × 22 m layouts (Figure 13b). The 32 × 20 m layout exhibits limited but noticeable pillar-edge damage (sloss < −0.15), while the 35 × 22 m layout shows even less damage, indicating better stability.

A similar pattern is observed in the weak rock mass strength case. Figure 14 (Stages 1 and 2) and Figure 15 (Stages 3 and 4) display sloss contours for the 32 × 20 m layout case, whereas Figure 16 (Stages 1 and 2) and Figure 17 (Stages 3 and 4) correspond to the 35 × 22 m layout case. Using sloss = −0.15 as a conservative failure depth threshold, the 32 × 20 m layout develops up to 6 m of damage, which would be severe enough to compromise footprint serviceability, whereas the 35 × 22 m layout limits failure depth to approximately 3 m, with damage mostly at pillar margins.

Overall, the results confirm the critical role of rock mass strength in determining the stability and serviceability of the cave footprint. In practice, rock mass strength within cave footprints exhibits a high degree of heterogeneity, with zones of both strong and weak ground distributed across the footprint. The impact of these variations on footprint stability depends on their location and the magnitude of stresses acting throughout the mine's lifespan. Therefore, stability assessments should consider the spatial distribution of these strength variations and the evolving stress conditions over time. That said, the wider-spaced layout shows better relative stability performance for both moderate and weak strength rock mass cases due to the larger size of the pillars.

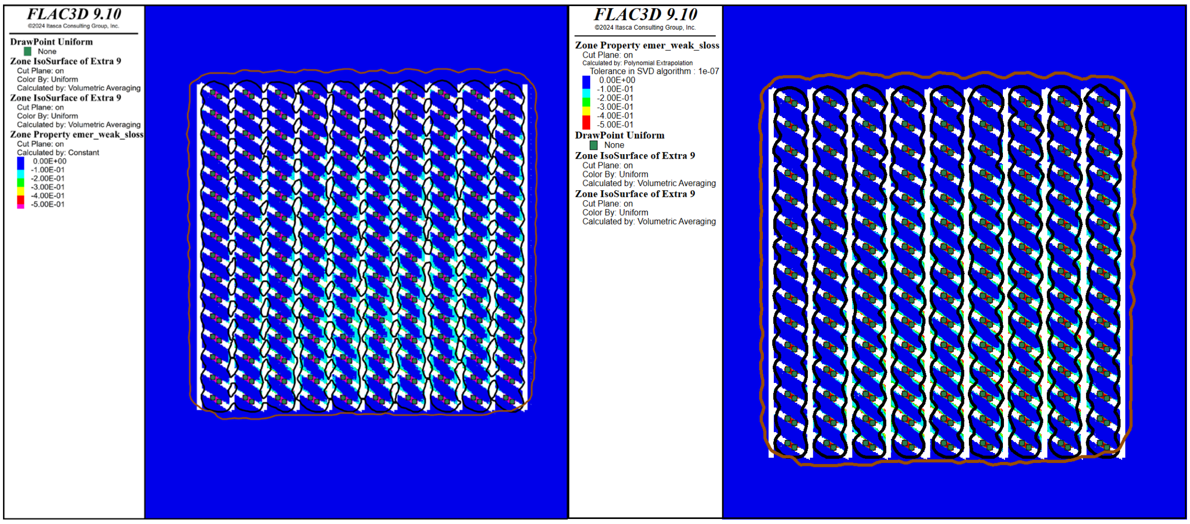

(a) (b)

Figure 13 Contour of sloss (between 0 and -0.5) at the end of Stage 4 with a moderate rock mass strength. (a) 32 × 20 m layout; (b) 35 × 22 m layout

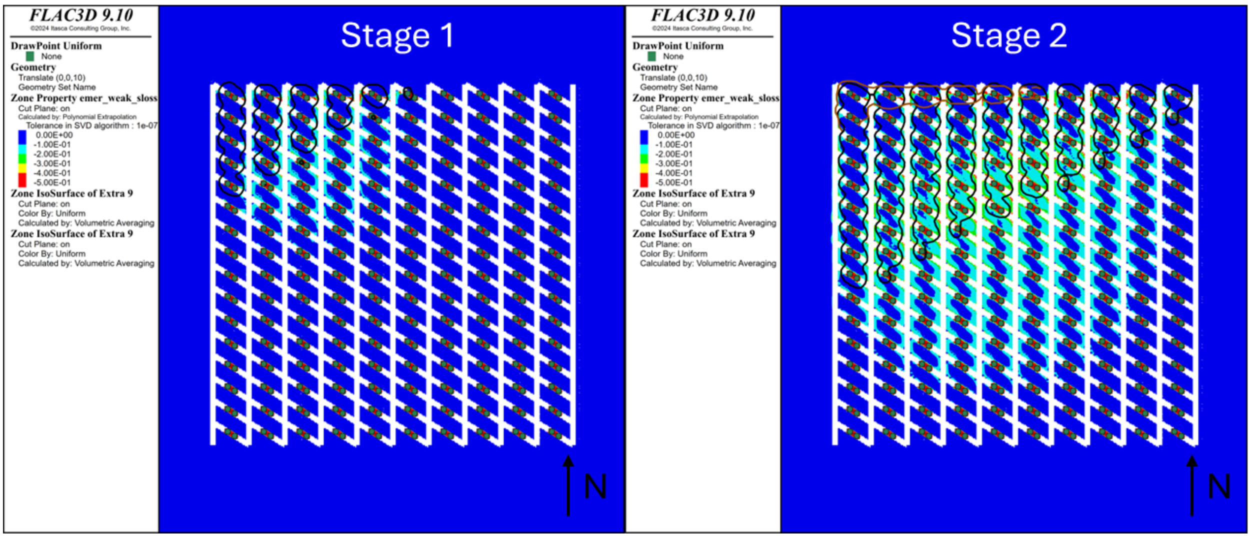

Figure 14 Contour of sloss (between 0 and -0.5) during Stage 1 (a) and Stage 2 (b)with a weak rock mass strength – 32 × 20 m layout

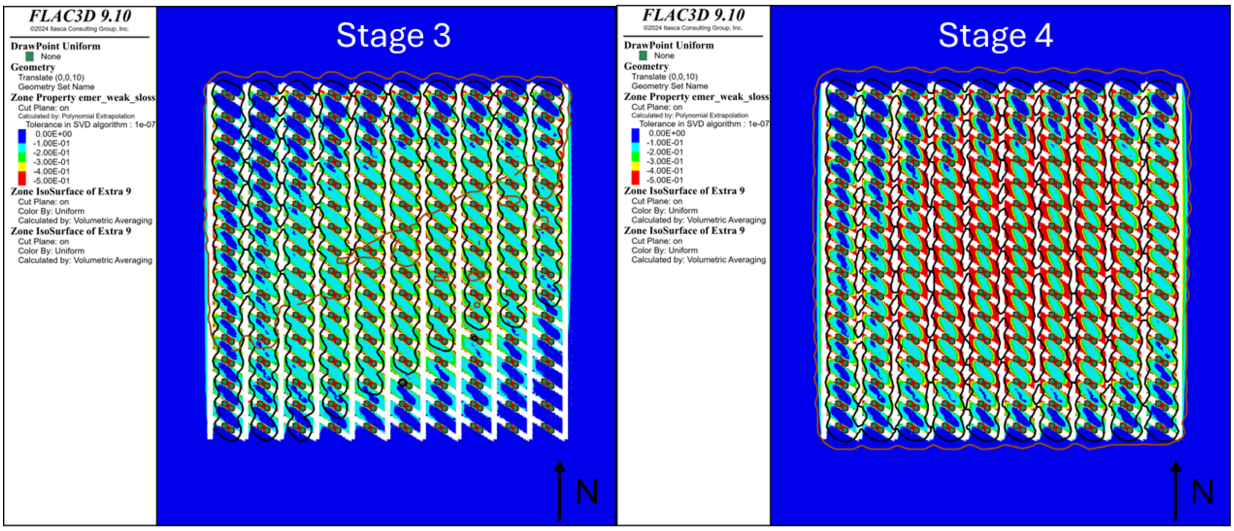

(a) (b)

Figure 15 Contour of sloss (between 0 and -0.5) during Stage 3 (a) and Stage 4 (b) with a weak rock mass strength – 32 × 20 m layout

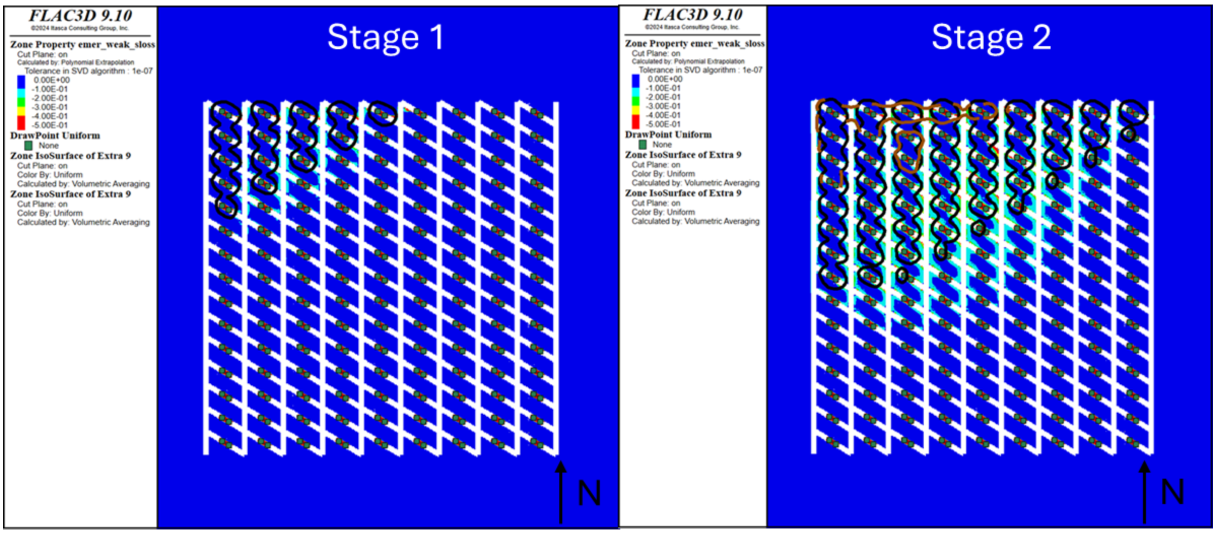

(a) (b)

Figure 16 Contour of sloss (between 0 and -0.5) during Stage 1 (a) and Stage 2 (b) with a weak rock mass strength – 35 × 22 m layout

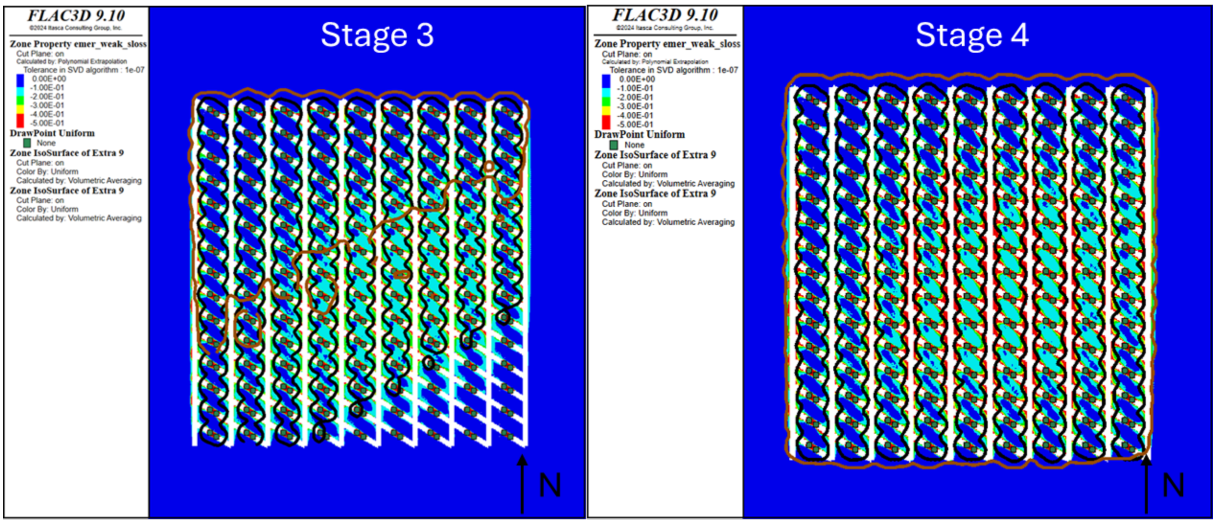

(a) (b)

Figure 17 Contour of sloss (between 0 and -0.5) during Stage 3 (a) and Stage 4 (b) with a weak rock mass strength – 35 × 22 m layout

4.2 Impact of draw strategy on abutment stress

The base case layout used a draw schedule based on PRC as per Figure 8. For the larger-pillar layout, two draw schedules with different PRCs were evaluated. The first draw schedule (35 × 22 m base case) used the same draw rate on a drawpoint basis (tpd/drawpoint) as the base case (32 × 20 m layout), while the second draw schedule (proportional draw) applied a draw rate proportional to the larger area of influence representative of the 35 × 22 m layout (i.e. used the same PRC from the 32 × 20 m case on a t/m^2/d basis), resulting in a 20% higher draw rate on a drawpoint basis (t/dp/d). A comparison between the base case production plan and a proportional draw plan was conducted to analyse the effect of draw rate on cave propagation as well as the impact of the induced stresses on the footprint.

In the case of the 35 × 22 m layout with a base draw rate (Figure 18), stress redistribution is slightly more pronounced compared to the 32 × 20 m layout (Figure 19), primarily due to the formation of pillars between isolated drawbells in the veranda zone. However, increasing the draw rate from the base to a higher draw rate (i.e. maintaining the same t/m²/day PRC as the 32 × 20 m layout) improves the connectivity of the undercut, reducing stress concentrations in the cave initiation zone and promoting better cave initiation. Under a higher draw rate, airgaps form a more continuous pattern in plan view, mitigating stress increases and enhancing cave propagation (Figure 20). This is relevant when assessing the scalability of design and planning variables with a larger spacing. It is worth noting that the effective draw rate applied to the drawpoints will depend on several factors, including materials handling capacity and interactions with other cave establishment activities, as well as airgap and cave angle management strategies.

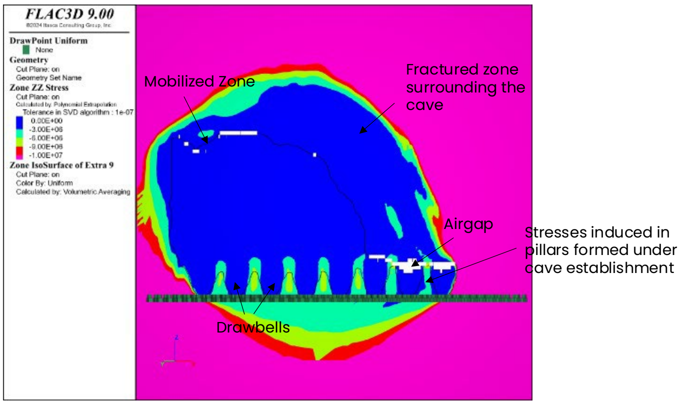

Figure 18 Distribution of vertical stress (Pa) inside the cave for 32 × 20 m layout (transverse section looking north)

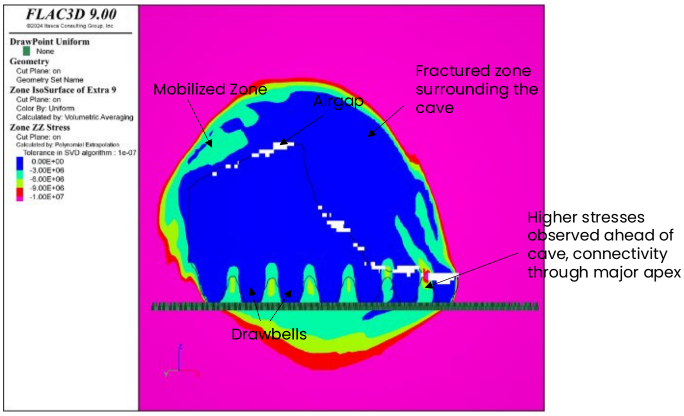

Figure 19 Distribution of vertical stress (Pa) inside the cave for 35 × 22 m layout – base draw rate (transverse section looking north)

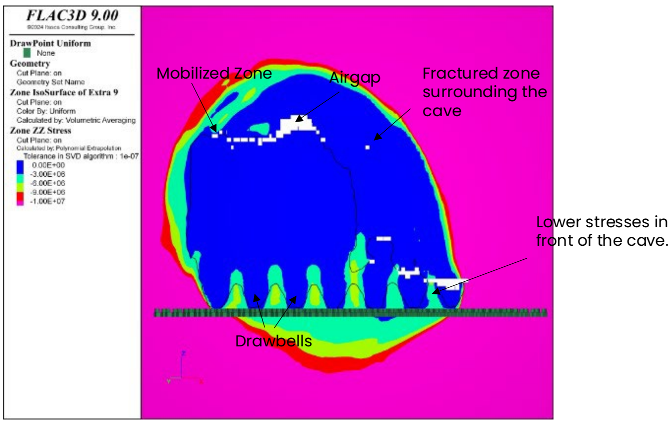

Figure 20 Distribution of vertical stress (Pa) inside the cave for 35 × 22 m layout – proportional draw rate (transverse section looking north)

4.3 Impact of time-induced compaction on cave loading and stability

To evaluate the impact of time-dependent compaction, draw was interrupted for 1 month in the central extraction drive after 200 weeks of continuous extraction (once the cave had reached an equivalent height of approximately 600 m); after this month, draw was resumed. Draw cessation of 1 month in an extraction drive is a likely scenario in a caving operation for different reasons, including concrete road replacements or extraction level maintenance.

The time-dependent compaction logic applied accounts for reduction in VSI (bulking factor) where the caved material remains stagnant due to draw cessation. This increases the strength and modulus of the material, causing it to act as a stress magnet. The resulting increase in vertical load (σzz) and sloss at the extraction level are shown in Figure 21 for the 32 × 20 m layout with moderate rock mass strength and in Figure 22 for the 35 × 22 m layout. Under these conditions, the increase in vertical load does not lead to significant changes in damage for both layouts, although the stress increase volume for the larger-pillar layout is larger. This is due to the larger pillars being able to absorb the stress increase better. For a weaker rock mass, the vertical load increase is more pronounced and may lead to future instabilities, even for the 35 × 22 m layout case (Figures 23).

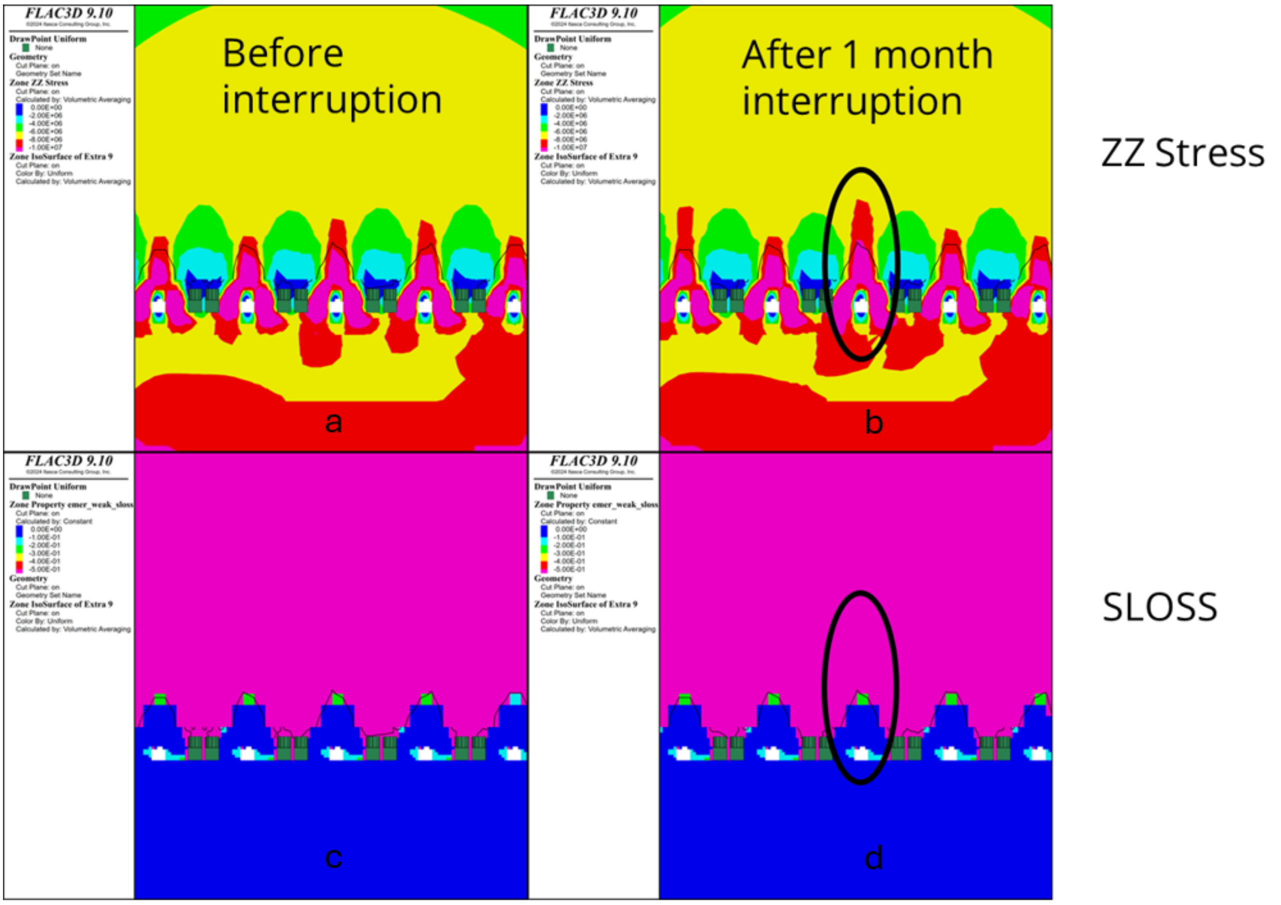

Figure 21 Vertical section showing induced vertical stress (σzz) on inactive extraction drive – 32 × 20 m layout before (a) and after (b) interruption – moderate strength. Vertical section showing contour of sloss on inactive extraction drive – 32 × 20 m layout before(c) and after (d) interruption – moderate strength

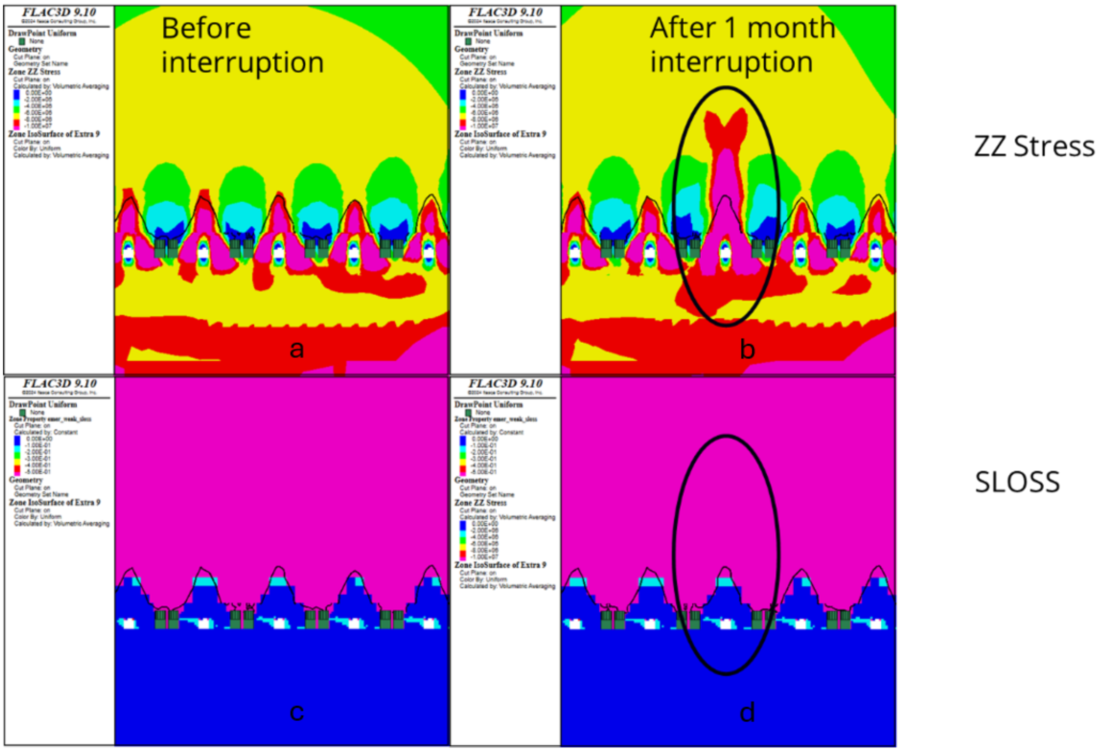

Figure 22 Vertical section showing induced vertical stress (σzz) on inactive extraction drive – 35 × 22 m layout before (a) and after (b) interruption – moderate strength. Vertical section showing contour of sloss on inactive extraction drive – 35 × 22 m layout before (c) and after (d) interruption – moderate strength

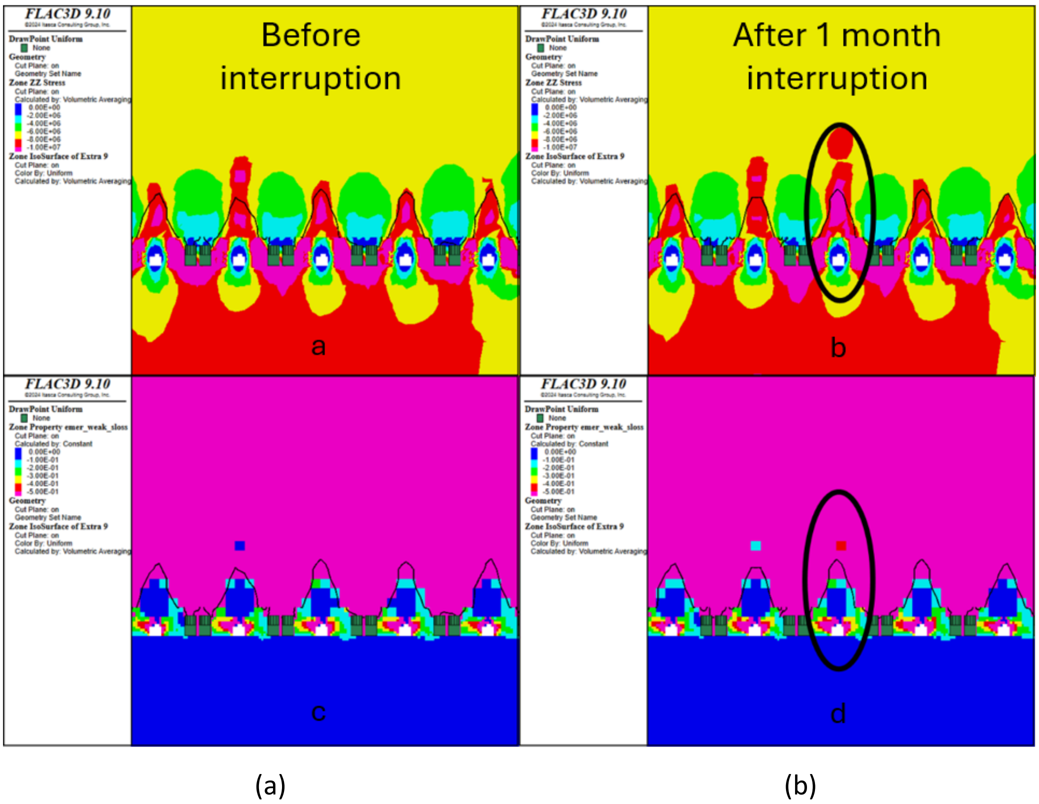

Figure 23 Vertical section showing induced vertical stress (zz) on inactive extraction drive – 35 × 22 m layout (a) before and (b) after interruption – weak strength. Vertical section showing contour of sloss on inactive extraction drive – 35 × 22 m layout (c) before and (d) after interruption – weak strength

5 Conclusion

In addition to recovery considerations, increasing spacing in the context of high-column caves introduces several system-level vulnerabilities, including a stronger dependence on uniform and continuous draw due to increased shear strain, fines generation and inrush susceptibility; reduced footprint productivity and operational redundancy resulting from fewer active drawpoints and drives; and heightened sensitivity to draw interruptions, which can accelerate stress loading, pillar damage and convergence. Furthermore, larger-pillar layouts require careful assessment of undercut height and connectivity to ensure early and continuous void formation, avoid remnant pillars, and prevent point loading on extraction level pillars, with draw strategy and geometric scaling guided by flow mechanics playing a critical role in achieving reliable cave initiation. Also, flow models have limitations in terms of the mechanisms they can reproduce, including effects of compaction and associated porosity changes, and analyses tend to be performed over idealised draw conditions. Therefore, detailed analysis, modelling and risk assessments need to be performed for the specific conditions of a given project before selecting the extraction level layout.

Importantly, increasing spacing increases the likelihood of large stagnant zones forming during undercutting and early cave establishment, particularly while draw zones remain isolated during ramp-up. If insufficient swell is removed, columns of compacted broken material may persist, transferring elevated sub-vertical stresses to the extraction level and creating stability risks. Current numerical modelling approaches do not fully capture these compaction-driven stress transfer mechanisms across the full life of the extraction level, highlighting a critical gap in design predictability. Addressing this gap is crucial for advancing the predictive capabilities of numerical models in block cave mining. Thus, this work aimed to investigate the effect of stress, compaction and spacing in high-column caves throughout the different stages of the life of the extraction level.

The methodology employed in the analysis effectively captures the loading cycle (changes in stress magnitude and orientation) experienced on the footprint during cave establishment and propagation.

During cave establishment, stresses are elevated in the cave initiation zone due to a larger tributary area developed in the pillar formed between leading drawbells. Under evaluated rock mass strength conditions, these elevated stresses do not cause additional substantial damage for the larger-pillar layout, as the larger pillar absorbs the increase in stress. This could vary depending on rock mass strength, presence of discontinuities and the stress environment. It is recommended to assess this based on the specific project's geotechnical environment.

Comparing footprint cumulative damage through cave maturity, the larger-pillar (35 × 22 m) footprint shows better conditions than the base case (32 × 20 m) layout. Damage is observed to concentrate in the abutments and static faces of the cave, where stresses are expected to be higher during cave propagation. This could vary depending on the geotechnical environment. Assessing this based on the specific project's geotechnical environment is recommended.

A comparison between the base case production plan and a proportional draw plan was conducted in order to analyse the effect of draw rate on cave propagation as well as the impact of the induced stresses on the footprint. The analysis concludes that increasing the draw rate on a t/m²/day basis improves the connectivity of the undercut, reducing stress concentrations in the cave initiation zone and promoting better cave initiation. Under a higher draw rate, airgaps form a more continuous pattern in plan, mitigating stress increases and enhancing cave propagation. Thus, the draw rate strategy and scalability need to be considered when increasing spacing to better manage cave propagation and stresses in the extraction level; however, as spacing increases, the system decreases the footprint productivity on a $t/m^2/d$ basis. This needs to be taken into consideration when designing a new block, as it can limit the drawpoint spacing.

In the case of draw interruption (1 month), an increase of vertical stress in the footprint is observed, corresponding to almost double the base vertical stress under no draw cessation, including the effect of compaction. The doubling of vertical stress does not cause a significant increase in damage for a moderate rock mass strength. This could vary depending on the geotechnical environment, as shown by the weak strength scenarios where significant damage as a result of draw interruption for both layout cases evaluated was observed. Also, draw interruptions due to planned activities and unplanned events in large block cave footprints are not uncommon, yet the geotechnical assessments usually assume ideal draw conditions throughout the entire life of the area. Assessing this as a sensitivity based on the specific project's geotechnical environment is recommended.

Future work should focus on incorporating more recent and representative research on the time-dependent compaction behaviour of caved rock masses, beyond the currently adopted Pancrudo slate results, and on calibrating these models through back-analysis of documented caved rock compaction case histories (e.g. Henderson mine) to enhance confidence in long-term cave response predictions.

Acknowledgement

The authors would like to acknowledge Matt Pierce for inspiring some of the ideas behind the study.

Disclaimer

The views and interpretations expressed in this paper reflect the independent research and interpretations of the authors, and do not necessarily represent the positions or endorsements of Newmont Corporation or its affiliates.

References

Cancino, C, Fuenzalida, MA & Kamp, C 2022, 'Modelling considerations for cave compaction at New Afton Mine', in Y Potvin (ed.), *Caving 2022: Proceedings of the Fifth International Conference on Block and Sublevel Caving*, Australian Centre for Geomechanics, Perth, pp. 573–582, https://doi.org/10.36487/ACG_repo/2205_39

Castro, R 2006, *The Study of the Mechanism of Gravity Flow for Block Caving*, PhD thesis, University of Queensland, Brisbane.

Castro, R, Vargas, R & De La Huerta, F 2012, 'Determination of drawpoint spacing in panel caving: a case study at the El Teniente Mine', *Journal of The Southern African Institute of Mining and Metallurgy*, vol. 112, pp. 871–876.

Cumming-Potvin, D, Wesseloo, J, Jacobsz, SW & Kearsley, E 2018, 'A re-evaluation of the conceptual model of caving mechanics', in Y Potvin & J Jakubec (eds), *Caving 2018: Proceedings of the Fourth International Symposium on Block and Sublevel Caving*, Australian Centre for Geomechanics, Perth, pp. 179–190, https://doi.org/10.36487/ACG_rep/1815_11_Cumming-Potvin

Fuenzalida, MA, Pierce, ME & Katsaga, T 2018, 'REBOP–FLAC3D hybrid approach to cave modelling', in Y Potvin & J Jakubec (eds), *Caving 2018: Proceedings of the Fourth International Symposium on Block and Sublevel Caving*, Australian Centre for Geomechanics, Perth, pp. 297–312, https://doi.org/10.36487/ACG_rep/1815_20_Pierce

Ghazvinian, E, Garza-Cruz, T, Bouzeran, L, Fuenzalida, M, Cheng, Z, Cancino, C & Pierce, M 2020, 'Theory and implementation of the Itasca constitutive model for advanced strain softening (IMASS)', in R Castro, F Báez & K Suzuki (eds), *MassMin 2020: Proceedings of the Eighth International Conference & Exhibition on Mass Mining*, University of Chile, Santiago, pp. 451–461.

Kwok, CY & Pierce, ME 2011, 'Time-dependent compaction in caving rock', *Proceedings, ARMA 45th US Rock Mechanics/Geomechanics Symposium*, American Rock Mechanics Association, Alexandria.

Kaiser, PK 2019, 'From common to best practices in underground rock engineering', Proceedings of the 14th ISRM Congress of Rock Mechanics, CRC Press, Boca Raton.

McDowell, GR & Bolton, MD 1998, 'On the micromechanics of crushable aggregates', *Geotechnique*, vol. 48, no. 5, pp. 667–679.

Morales, D, Henríquez, JP & Castro, R 2024, 'Methodology to determine the undercut height in Block/Panel Caving ', in Daniel Johansson & Håkan Schunnesson (eds), *MassMin 2024: Proceedings of the International Conference & Exhibition on Mass Mining*, Luleå University of Technology, Luleå, pp. 164–182, https://doi.org/10.36487/ACG_repo/2435_A-15

Oldecop, LA & Alonso, EE 2007, 'Theoretical investigation of the time-dependent behaviour of rockfill', *Geotechnique*, vol. 57, no. 3, pp. 289–301.

Pappas, D & Mark, C 1993, *Behavior of Simulated Longwall Gob Material. Report of Investigations*, 9458 USBM.

Paredes, P 2022, 'Evaluation of the effect of wider-spaced layouts in recovery for high column block caves', in Y Potvin (ed.), *Caving 2022: Proceedings of the Fifth International Conference on Block and Sublevel Caving*, Australian Centre for Geomechanics, Perth, pp. 393–416, https://doi.org/10.36487/ACG_repo/2205_27

Pierce, ME 2018, 'Forecasting vulnerability of deep extraction level excavations to draw-induced cave loads', *Journal of Rock Mechanics and Geotechnical Engineering*, vol. 11, no. 3, pp. 527–534.

Shea, NA, Sinclair, RW & Welsh, TM 2018, 'Safely re-opening a collapsed extraction level drive in a resource-limited environment', in Y Potvin & J Jakubec (eds), *Caving 2018: Proceedings of the Fourth International Symposium on Block and Sublevel Caving*, Australian Centre for Geomechanics, Perth, pp. 45–56, https://doi.org/10.36487/ACG_rep/1815_01_Shea